IEEE Access
Multidisciplinary | Rapid Review | Open Access Journal

Received January 28, 2021, accepted February 7, 2021, date of publication February 26, 2021, date of current version March 8, 2021.

Digital Object Identifier 10.1109/ACCESS.2021.3062449

Rapid Multi-Criterial Antenna Optimization by Means of Pareto Front Triangulation and Interpolative Design Predictors

SLAWOMIR KOZIEL[1,2], (Senior Member, IEEE), AND ANNA PIETRENKO-DABROWSKA[2], (Senior Member, IEEE)

[1]Engineering Optimization & Modeling Center, Department of Technology, Reykjavik University, 102 Reykjavik, Iceland
[2]Faculty of Electronics, Telecommunications and Informatics, Gdańsk University of Technology, 80-233 Gdańsk, Poland

Corresponding author: Anna Pietrenko-Dabrowska (anna.dabrowska@pg.edu.pl)

This work was supported in part by the Rannsóknamiðstöð Íslands (RANNIS) under Grant 217771051, and in part by the National Science Centre of Poland under Grant 2020/37/B/ST7/01448.

ABSTRACT Modern antenna systems are designed to meet stringent performance requirements pertinent to both their electrical and field properties. The objectives typically stay in conflict with each other. As the simultaneous improvement of all performance parameters is rarely possible, compromise solutions have to be sought. The most comprehensive information about available design trade-offs can be obtained through multi-objective optimization (MO), typically in the form of a Pareto set. Notwithstanding, MO is a numerically challenging task, in a large part due to high CPU cost of evaluating the antenna properties, normally carried out through full-wave electromagnetic (EM) analysis. Surrogate-assisted procedures can mitigate the cost issue to a certain extent but construction of reliable metamodels is hindered by the curse of dimensionality, and often highly nonlinear antenna characteristics. This work proposes an alternative approach to MO of antennas. The major contribution of our work consists in establishing a deterministic machine learning procedure, which involves sequential generation of Pareto-optimal designs based on the knowledge gathered so far in the process (specifically, by triangulation of the already obtained Pareto set), and local surrogate-assisted refinement procedures. Our methodology allows for rendering uniformly-distributed Pareto designs at the cost of a few hundreds of antenna EM simulations, as demonstrated by means of three verification case studies. Benchmarking against state-of-the-art MO techniques is provided as well.

INDEX TERMS Antenna optimization, EM-driven design, multi-criterial design, Pareto front triangulation, surrogate modeling.

I. INTRODUCTION

Contemporary antenna systems have to satisfy multiple and often stringent requirements concerning their electrical and field characteristics, such as broadband [1] or multi-band operation [2], multi-input multi-output (MIMO) functionality [3], circular polarization [4], tunability [5], pattern diversity [6], or enhanced gain [7]. These specifications are rooted in the needs pertinent to specific application areas (e.g., wearable [8] or implantable devices [9]), including the emerging technologies such as 5G [10]–[12], or the internet of things (IoT) [13], [14]. Their fulfilment generally requires novel and complex antenna structures, whose geometries are parameterized by large numbers of variables, when compared to traditional radiators [15]–[17]. Appropriate tuning of antenna dimensions is critical from the point of view of achieving satisfactory levels of performance parameters. On the other hand, it is a challenging process due to high computational cost of antenna evaluation, normally realized using electromagnetic (EM) analysis. The necessity of handling multiple goals and constraints only aggravates the problem. Furthermore, as the design objectives are often conflicting (i.e., the improvement of one results in a degradation of others), trade-off solutions need to be identified. Perhaps the most common example is the design of compact antennas, where diminishing the antenna size leads to various undesirable effects (e.g., a reduction of the impedance bandwidth, loss of efficiency, and pattern stability, etc. [18], [19]).

The associate editor coordinating the review of this manuscript and approving it for publication was Liang-Bi Chen.

Given the aforementioned issues, it is clear that conventional, yet still widespread EM-driven design methods (primarily those relying on parametric studies) are grossly incapable of handling complex design scenarios, particularly those involving multiple objectives. Numerical optimization procedures are much more suitable for this purpose [20]; yet, the vast majority of available algorithms, both conventional (gradient-based methods [21], pattern search [22]), and nature-inspired (evolutionary algorithms [23], differential evolution [24], particle swarm optimizers [25], firefly algorithm [26]) can only process scalar objective functions. For practical convenience, multi-objective tasks are often reformulated into single-objective ones using, e.g., weighted sum method [27] or goal attainment approach [28], as well as objective prioritization by selecting a primary goal and turning the others into constraints [29]. This allows for utilization of the standard algorithmic approaches. At the same time, the obtained solutions are biased towards the user priorities concerning the design goals.

In order to generate more complete information about the best possible design trade-offs, typically in the form of a Pareto set, a proper multi-objective optimization (MO) is necessary [30]. In principle, single-objective routines can be adopted for this purpose, e.g., by means of executing repetitive optimization of the aggregated objectives with variable weighting factors [27]. Notwithstanding, the most widely used algorithms nowadays are nature-inspired population-based procedures mimicking either biological [31] or social phenomena [32], many of which have their multi-objective versions. Some of the popular methods include evolutionary algorithms [33], differential evolution [34], particle swarm optimization [35], invasive weed optimization [36], ant colony [37], and others [38], [39]. The most important benefit of population-based procedures is the ability of rendering the entire Pareto set in on algorithm run. On the other hand, the practical bottleneck is poor computational efficiency with usually thousands of objective function evaluations required to converge. Clearly, such a cost may be prohibitive if the antenna under design is evaluated using full-wave EM analysis.

One of possible ways to alleviate the cost-related difficulties is to combine population-based methods with surrogate modeling techniques [40], [41]. In some cases, a construction of the surrogate may be possible within the entire parameter space of the problem at hand; however, it only applies to relatively simple and low-dimensional problems [42], [43]. In the case of antennas, an additional obstacle is highly nonlinear dependence between the geometry parameters and the system outputs [44]. Furthermore, as mentioned before, majority of modern antennas are described by a relatively large number of parameters (typically, over ten). A workaround is the application of machine learning techniques where rendering of the surrogate is interleaved with the prediction stages, at which the promising regions of the space are identified, and the surrogate models are iteratively improved therein using various infill criteria [45], [46]. Popular modeling methods utilized within these frameworks include kriging [47], Gaussian process regression [48], and support vector machines [49]. Another possibility is the application of variable-fidelity EM simulations [41]. Finally, it is also possible to employ performance-driven modeling techniques, where the surrogate model domain is confined to the regions containing high-quality designs, and the training data is only acquired therein [50]. Performance-driven models have been adopted for MO purposes and demonstrated to be efficient for handling multi-parameter antenna structures [51], [52].

The techniques mentioned in the previous paragraphs are stochastic in the sense that at some stage of the optimization process, randomized search procedures (in particular, nature-inspired methods) are employed, either to handle the problem objectives directly or at the level of the surrogate model. Recently, several deterministic surrogate-assisted MO techniques have been proposed including point-by-point Pareto front exploration [53], a bisection method [54], as well as sequential domain patching (SDP) [55]. Although these algorithms have been developed to handle two-objective problems, some generalized versions have been proposed as well (generalized bisection [56], or generalized SDP [57]). A common feature of the mentioned techniques is a sequential generation of Pareto-optimal designs by iterative adjustment of design specifications and solving local constrained minimization tasks, either directly [54] or using local surrogates [53]. Perhaps the most important advantage of such methods is that no globally accurate replacement models have to be constructed (in other words, the method exhibits immunity against dimensionality issues) and no stochastic search algorithm have to be involved.

This paper proposes a novel deterministic machine-learning-based framework for multi-objective design optimization of antenna structures. Our methodology involves the already gathered knowledge about the system at hand in the form of currently available Pareto-optimal set, triangulation of the latter and interpolative predictors employed to generate the infill points, as well as local design refinement procedures to obtain additional optimum points. The presented approach is generic in the sense of being able to handle arbitrary number of objectives, and allows for generating uniformly distributed Pareto sets. Furthermore, it is computationally efficient as demonstrated using three antenna structures, an ultra-wideband (UWB) monopole optimized for minimum size and minimum in-band reflection, a quasi-Yagi antenna optimized for maximum end-fire gain and minimum reflection, as well as an UWB antenna optimized for three objectives: minimum size, minimum reflection, and minimum in-band gain variability. In all cases, the sets of trade-off designs are rendered at the cost of a few hundreds of EM analyses of the respective antennas. Benchmarking against surrogate-assisted methods is also provided, showing that the presented approach enables considerable savings but also improved uniformity of the Pareto set.

II. MULTI-OBJECTIVE ANTENNA DESIGN VIA PARETO SET TRIANGULATION

This section introduces the multi-objective optimization procedure proposed in the paper. We start by recalling the formulation of the MO task, followed by the discussion of the Pareto set triangulation and the iterative procedure of generating new Pareto-optimal points by using a predictor constructed over the existing designs and local constrained refinement. Demonstration case studies and benchmarking will be presented in Section III.

A. MULTI-OBJECTIVE ANTENNA OPTIMIZATION. PARETO SET

The design objectives, all to be minimized, are denoted as F_k, $k = 1, \ldots, N_{obj}$. The goal of multi-objective optimization, as understood in this paper, is to identify a set of globally non-dominated designs or a Pareto set, which is a discrete representation of the Pareto front, i.e., the best possible trade-offs between the objectives F_k. The definition of the dominance relation can be found in the vast literature of the subject (e.g., [58]). In plain words, a globally non-dominated design $\boldsymbol{x}$ is such that no other design exists within the considered parameter space X that is better than $\boldsymbol{x}$ with respect to all objectives simultaneously. One of the consequences is that all Pareto set elements are equally good regarding the objective vector $\boldsymbol{F} = [F_1\ F_2 \ldots F_{Nobj}]^T$.

The antenna structure under design is assumed to be evaluated through full-wave EM analysis. The output of the computational model (e.g., relevant frequency characteristics) will be denoted as $\boldsymbol{R}(\boldsymbol{x})$ with $\boldsymbol{x}$ being a vector of (usually geometry) parameters to be adjusted. The introductory part of the paper briefly discussed possible ways of mitigating the issue related to high computational cost of massive EM simulations required by conventional MO algorithms. These include both the hybrid approaches, primarily combinations of nature-inspired algorithms and surrogate modeling methods [41]–[45], deterministic algorithms [56], [59], as well as multi-fidelity methodologies combined with the refinement strategies [40].

B. PARETO SET TRIANGULATION. INVERSE SURROGATE

The major underlying assumption for the MO procedure proposed in this paper is that the Pareto front is a connected set, both in the parameter space X, and the space of design objectives F. This means, in particular, that it does not contain several disjoint subsets. For many practical antenna MO tasks, this sort of condition is satisfied and follows from the continuity of antenna characteristics as a function of the designable parameters.

For the purpose of our considerations, let $\boldsymbol{x}^{(k)}$, $k = 1,\ldots, p$, denote the Pareto-optimal designs found so far in the MO process, and $\boldsymbol{F}^{(k)} = \boldsymbol{F}(\boldsymbol{x}^{(k)}) = [F_1^{(k)} \ldots F_{Nobj}^{(k)}]^T$ be the corresponding objective vectors. The first N_{obj} designs are the single-objective optima

$$\boldsymbol{x}^{(k)} = \arg\min_{\boldsymbol{x}\in X} F_k\left(\boldsymbol{R}(\boldsymbol{x})\right) \tag{1}$$

These points (extreme Pareto-optimal designs [40]) determine the span of the Pareto front. Subsequent points are iteratively determined as elaborated on below.

Further, let $\boldsymbol{s}(\boldsymbol{F})$: $F \rightarrow X$ be the inverse surrogate established using the training data $\{\boldsymbol{F}^{(k)}, \boldsymbol{x}^{(k)}\}_{k=1,\ldots,p}$. The model is referred to as inverse because its codomain is the antenna parameter set. In our approach the inverse surrogate $\boldsymbol{s}(\boldsymbol{F})$ is utilized to generate the predictions about the Pareto-optimal designs parameterized using the objectives F_k, $k = 1, \ldots, N_{obj}$. In other words, the inverse surrogate renders an initial design for finding a new Pareto-optimal design. In this work, the data-driven surrogate is constructed using kriging interpolation [46] although other modelling techniques can be used as well.

Let $\boldsymbol{S}^{(j)}$, $j = 1, \ldots, K_p$, be the simplexes obtained by triangulation of the set $\{\boldsymbol{F}^{(k)}\}_{k=1,\ldots,p}$. The simplex vertices in the objective space are $\boldsymbol{S}^{(j)} = \{\boldsymbol{F}^{(j.1)}, \ldots, \boldsymbol{F}^{(j.Nobj)}\}$, with $\boldsymbol{F}^{(j.r)} \in \{\boldsymbol{F}^{(k)}\}_{k=1,\ldots,p}$, for $r = 1, \ldots, N_{obj}$. We use Delaunay triangulation to avoid near-to-degenerate simplexes.

C. GENERATING PARETO-OPTIMAL DESIGNS BY INVERSE SURROGATE. DESIGN REFINEMENT

The simplexes determine the partitioning of the current representation of the Pareto set, and are used to allocate a new point, which is realized in the form of machine-learning algorithm according to the sequential design of experiments strategy based on Delaunay triangulation [60]. In particular, if $A(\boldsymbol{S}^{(j)})$ denotes the volume of the simplex $\boldsymbol{S}^{(j)}$, the new (temporary) objective vector is allocated as

$$\boldsymbol{F}_{tmp} = \frac{1}{N_{obj}} \sum_{k=1}^{N_{obj}} \boldsymbol{F}^{(j_{\max}.k)} \tag{2}$$

where

$$j_{\max} = \arg\max_{1\le j\le N_{obj}} \{A(\boldsymbol{S}^{(j)})\} \tag{3}$$

In other words, $\boldsymbol{F}_{tmp} = [F_{tmp.1} \ldots F_{tmp.Nobj}]^T$ is the center of the simplex having the largest volume among the set $\boldsymbol{S}^{(j)}$, $j = 1, \ldots, K_p$.

The initial design $\boldsymbol{x}_{tmp}$ used to find a new Pareto-optimal design is then assigned as the image of the vector $\boldsymbol{F}_{tmp}$ through the surrogate $\boldsymbol{s}$, i.e.,

$$\boldsymbol{x}_{tmp} = \boldsymbol{s}(\boldsymbol{F}_{tmp}) \tag{4}$$

As an additional precaution, an alternative initial design is generated as the center of the simplex $\boldsymbol{S}^{(j\max)}$ in the parameter space, i.e.,

$$\boldsymbol{x}_{tmp.alt} = \frac{1}{N_{obj}} \sum_{k=1}^{N_{obj}} \boldsymbol{x}^{(j_{\max}.k)} \tag{5}$$

where $\boldsymbol{x}^{(j_{\max}.k)}$, $k = 1, \ldots, N_{obj}$, is the parameter space vector corresponding to $\boldsymbol{F}^{(j_{\max}.k)}$. Effectively, the design $\boldsymbol{x}_{tmp.alt}$ is obtained in the same way as (4) but using the linear model established using the (parameter space) vertices of the simplex $\boldsymbol{S}^{(j_{\max})}$. Having both $\boldsymbol{x}_{tmp}$ and $\boldsymbol{x}_{tmp.alt}$, the better of the two (in terms of the smaller value of the objective F_1) is selected

as the initial design. The reason for considering the alternative initial design is that at certain stages of the optimization process, the prediction of the kriging surrogate model **s** may be of limited reliability. For example, the surrogate accuracy may be questionable at locations in between already found Pareto-optimal points being relatively away from each other, while other points are located close to their neighbors (with the latter determining the surrogate hyper-parameter values).

Because the inverse surrogate only provides an approximation of the Pareto front, the design $\boldsymbol{x}_{tmp}$ has to be refined in order to be "pushed" towards the front. This is realized by solving the following single-objective task

$$\boldsymbol{x}^{(p+1)} = \begin{array}{c} \arg\min \\ \boldsymbol{x},\ F_2(\boldsymbol{x}) \le F_{tmp.2} \\ \vdots \\ F_{N_{obj}}(\boldsymbol{x}) \le F_{tmp.N_{obj}} \end{array} F_1\left(\boldsymbol{R}(\boldsymbol{x})\right) \quad (6)$$

In (6), the goal is to improve the first objective as much as possible while fulfilling constraints imposed on the remaining ones, as determined by the initial vector $\boldsymbol{F}_{tmp}$. The problem (6) is solved using a local procedure, specifically, trust-region-embedded gradient search, which generates approximations $\boldsymbol{x}^{(p+1.i)}$, $i = 0, 1, \ldots$, to $\boldsymbol{x}^{(p+1)}$ (with $\boldsymbol{x}^{(p+1.0)} = \boldsymbol{x}_{tmp}$) as

$$\boldsymbol{x}^{(p+1.i+1)} = \begin{array}{c} \arg\min \\ \boldsymbol{x},\ \boldsymbol{x}^{(p+1.i)} - \boldsymbol{d}^{(i)} \le \boldsymbol{x} \le \boldsymbol{x}^{(p+1.i)} + \boldsymbol{d}^{(i)} \\ F_2(\boldsymbol{x}) \le F_{tmp.2} \\ \vdots \\ F_{N_{obj}}(\boldsymbol{x}) \le F_{tmp.N_{obj}} \end{array} F_1\left(\boldsymbol{L}^{(i)}(\boldsymbol{x})\right) \quad (7)$$

where $\boldsymbol{L}^{(i)} = \boldsymbol{R}(\boldsymbol{x}^{(p+1.i)}) + \boldsymbol{J}_{\boldsymbol{R}}(\boldsymbol{x}^{(p+1.i)}) \cdot (\boldsymbol{x} - \boldsymbol{x}^{(p+1.i)})$. The sensitivity matrix $\boldsymbol{J}_{\boldsymbol{R}}$ is estimated using finite differentiation in the first iteration, and then updated using the Broyden formula [61]. Rank-one updates are sufficient because the initial design $\boldsymbol{x}_{tmp}$ is normally close to the refined one, and the prediction accuracy of the surrogate (cf. (4)) is expected to improve as the distances between the existing designs $\boldsymbol{x}^{(k)}$ become smaller. Figure 1 shows a graphical illustration of the considered concepts.

The new Pareto-optimal point $\boldsymbol{x}^{(p+1)}$ is incorporated into the existing representation of the Pareto set to create the updated training ensemble $\{\boldsymbol{F}^{(k)}, \boldsymbol{x}^{(k)}\}_{k=1,\ldots,p+1}$. The latter is used to re-generate the surrogate model $\boldsymbol{s}(\boldsymbol{F})$, which concludes the iteration of the algorithm. The procedure is terminated when the required number of designs along the front have been identified.

D. OPTIMIZATION PROCEDURE

The proposed multi-objective optimization procedure has been summarized in the form of the flow diagram shown in Fig. 2. The optimization process starts by acquiring the single-objective optima $\boldsymbol{x}^{(k)}$, $k = 1, \ldots, N_{obj}$ (extreme Pareto-optimal designs) as discussed in Section II. *B* (cf. (1)).

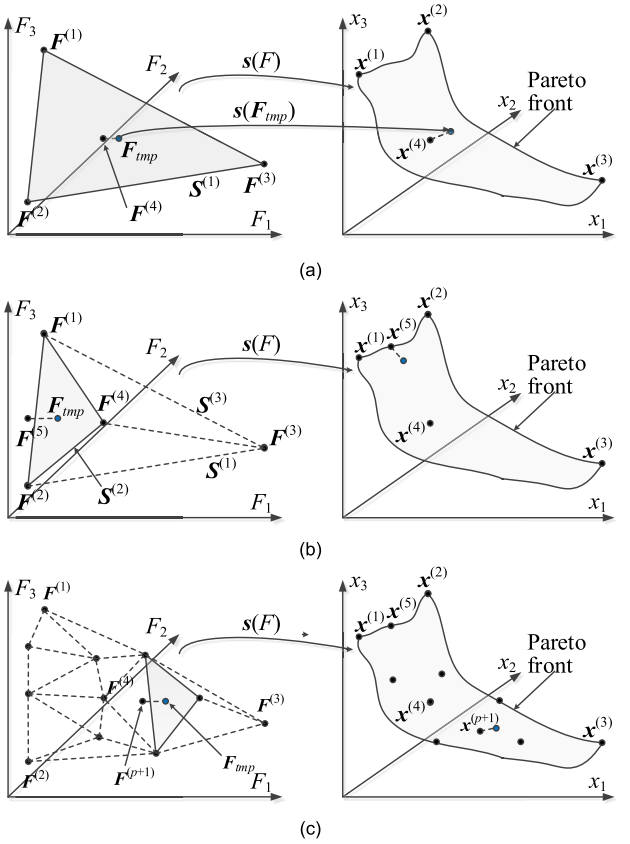

FIGURE 1. Knowledge-based multi-objective design by Pareto front triangulation: conceptual illustration. The left panel shows the objective space (here, three dimensional), whereas the right panel illustrates the parameter space (here, also three-dimensional): (a) first iteration: the extreme Pareto-optimal designs $\boldsymbol{F}_k$, $k = 1, 2, 3$, are triangulated in the objective space to produce the initial point $\boldsymbol{s}(\boldsymbol{F}_{tmp})$; this design is refined (cf. (5), (6)) to obtain the new Pareto-optimal point $\boldsymbol{x}^{(4)}$ and its representation in the objective space $\boldsymbol{F}^{(4)}$; (b) second iteration of the algorithm, where the initial (objective space) design $\boldsymbol{F}_{tmp}$ is allocated in the center of the largest simplex (here, $\boldsymbol{S}^{(2)}$); (c) one of the further iterations of the procedure.

Using this data, the initial surrogate model $\boldsymbol{s}(\boldsymbol{F})$ is constructed and utilized to generate the initial design $\boldsymbol{x}_{tmp}$, following triangulation of the existing representation of the Pareto set in the objective space and identification of the largest simplex $\boldsymbol{S}^{(j\max)}$. The refinement process (6), (7) involves a solution to the constrained problem aiming at the improvement of the first objective without degrading the remaining ones, which pushes the design towards the Pareto front. The computational cost of this operation is low due to using a trust-region gradient-based algorithm with sparse sensitivity updates and availability of good initial design, the quality of which is gradually improving once the size of the existing Pareto set increases. The procedure is terminated upon finding the required number of designs.

It should be emphasized that the considered MO algorithm is fully deterministic, it does not require any auxiliary stochastic search procedures, and its computational cost can be estimated beforehand based on the target number of Pareto optimal designs to be generated. Furthermore, the knowledge

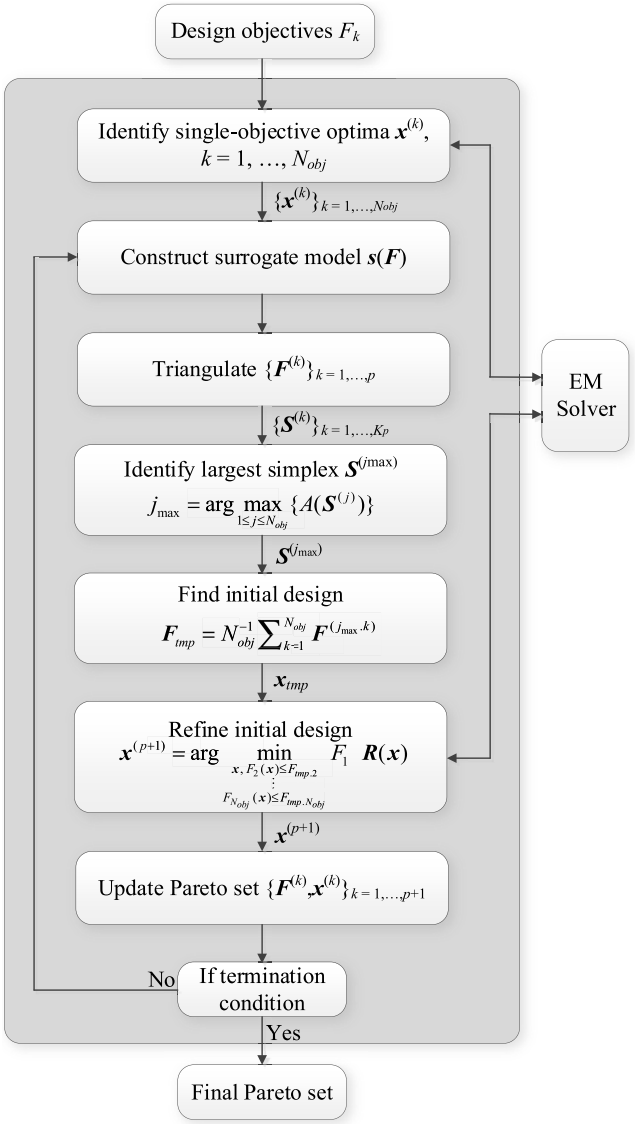

FIGURE 2. Flow diagram of the proposed machine-learning-based framework for multi-objective optimization of antennas by Pareto front triangulation and interpolative predictors.

about the trade-off designs that have been acquired at any given stage of the search process is fully exploited using machine learning (here, inverse surrogates).

An additional benefit that follows directly from the formulation of the method is a fairly uniform coverage of the Pareto front that can be rendered. As mentioned before, there are certain limitations as well. The major assumption is that the Pareto front is a connected set in the parameter space, i.e., it does not contain several disjoint regions. Although this is not always the case, the assumption would normally hold of many practical antenna cases because of continuous dependence between antenna dimensions and frequency characteristics [40].

III. VERIFICATION CASE STUDIES AND BENCHMARKING

This section provides numerical verification of the multi-objective optimization framework introduced in Section II.

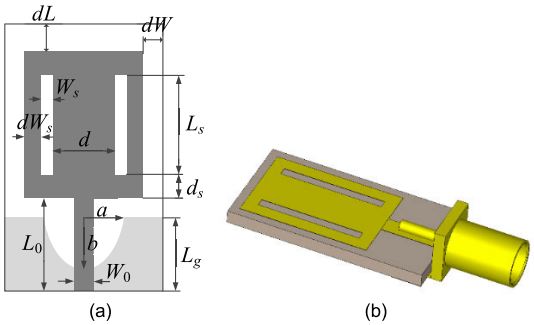

FIGURE 3. Ultra-wideband monopole antenna with radiator slots: (a) antenna geometry with the ground plane marked using the light-gray shade, (b) perspective view.

Demonstration case studies include three antenna structures: two ultra-wideband monopoles, and a planar Yagi antenna. Two of these structures are optimized for two objectives (the first monopole and the Yagi antenna), the third one is designed with respect to three objectives. The design goals include size reduction, matching improvement, as well as reduction of the in-band gain variability. For the sake of benchmarking, a surrogate-assisted procedure involving initial parameter range reduction, a population-based metaheuristic algorithm, and response correction algorithm for design refinement, is utilized. In all cases, the considered algorithms exclusively use high-fidelity EM simulations.

A. EXAMPLE 1: ULTRA-WIDEBAND MONOPOLE ANTENNA WITH RADIATOR SLOTS

Our first example is an ultra-wideband (UWB) monopole with two radiator slots [62], shown in Fig. 3. The antenna is implemented on FR4 substrate ($\varepsilon_r = 4.3$, $h = 1.55$ mm). The independent parameters are $\boldsymbol{x} = [L_g L_0 L_s W_s d\ dL\ d_s\ dW_s\ dW\ a\ b]^T$. The feeding line width $W_0 = 2.0$ mm is fixed to ensure 50 ohm input impedance (the unit for all parameters is mm). The EM model is implemented in CST Microwave Studio (~600,000 mesh cells, simulation time 3 minutes). In this work, all the simulations were performed on Intel Xeon 2.1 GHz dual-core CPU, 128 GB RAM. The computational model includes the SMA connector.

For the antenna of Fig. 3, we consider two objectives: F_1 – minimization of maximum reflection over the frequency range 3.1 GHz to 10.6 GHz, and F_2 – minimization of antenna footprint $A(\boldsymbol{x}) = (a+2o)(l_0+l_1+w_1)$. We are only interested in the part of the Pareto front for which the maximum in-band reflection does not exceed the level of around −10 dB.

The single-objective optima have been found using trust-region gradient search [63]: $\boldsymbol{x}^{(1)} = [9.07\ 13.39\ 9.93\ 0.43\ 2.03\ 9.17\ 0.80\ 2.29\ 3.02\ 0.29\ 0.59]^T$ mm (the best matching design), $\boldsymbol{x}^{(2)} = [9.81\ 13.26\ 7.82\ 0.23\ 4.36\ 0.00\ 0.97\ 1.20\ 0.00\ 0.80\ 0.62]^T$ mm (the minimum size design).

Figure 4 shows the 10-element Pareto set obtained using the methodology of Section 2. Table 1 shows the breakdown of the computational cost of the optimization process.

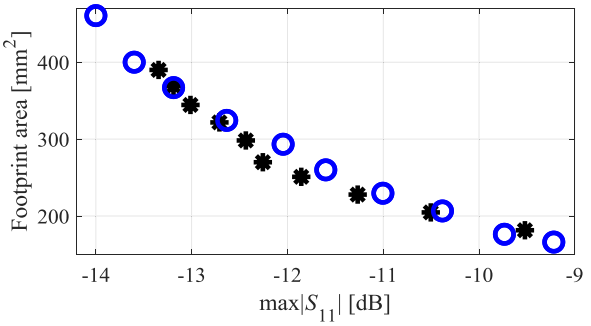

FIGURE 4. UWB monopole antenna of Fig. 3: Pareto set found by means of the proposed methodology (o), and the set identified using the surrogate-assisted technique of [40] (*).

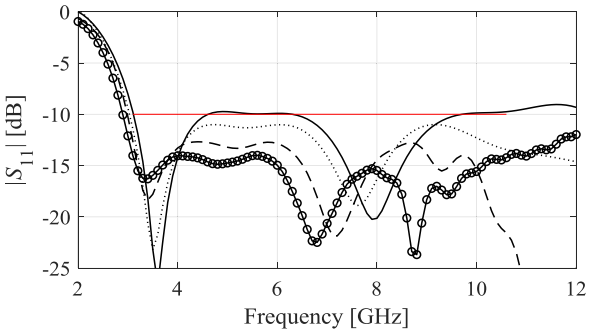

FIGURE 5. UWB monopole antenna of Fig. 3: reflection responses at selected Pareto-optimal designs of Table 2: $\boldsymbol{x}^{(2)}$ (—), $\boldsymbol{x}^{(4)}$ (· · ·), $\boldsymbol{x}^{(7)}$ (- - -), and $\boldsymbol{x}^{(10)}$ (-o-).

TABLE 1. UWB antenna of Fig. 3: optimization cost and benchmarking.

This work (inverse modeling & refinement)		Surrogate-assisted procedure [40] (benchmark)	
Cost item	Cost[#]	Cost item	Cost[#]
Single-objective optimization runs (designs $\boldsymbol{x}^{(1)}$ and $\boldsymbol{x}^{(2)}$)	$403 \times \boldsymbol{R}$	Single-objective optimization runs (designs $\boldsymbol{x}^{(1)}$ and $\boldsymbol{x}^{(2)}$)	$403 \times \boldsymbol{R}$
		Data acquisition for kriging surrogate	$1000 \times \boldsymbol{R}$
Design refinement	$162 \times \boldsymbol{R}$	MOEA optimization*	N/A
		Design refinement	$30 \times \boldsymbol{R}$
Total cost[#]	$575 \times \boldsymbol{R}$ (29 h)	Total cost[#]	$1433 \times \boldsymbol{R}$ (72 h)

* The cost of MOEA optimization is negligible compared to other stages of the process.
[#] The cost is expressed in terms of the equivalent number of EM simulations (marked as $\times \boldsymbol{R}$).

The cost of generating the designs $\boldsymbol{x}^{(1)}$ and $\boldsymbol{x}^{(2)}$ is 403 EM antenna simulations, whereas the expenses related to the acquisition of the remaining designs is only 162 simulations. Thus, the total cost is 575 EM antenna simulations (or only 20 simulations per design when excluding extreme Pareto-optimal point generation). Figure 4 and Table 1 also show the results obtained using the benchmark technique, which is a surrogate-assisted framework [40], where the kriging surrogate model is constructed in the interval $[\boldsymbol{l}^* \ \boldsymbol{u}^*]$ with $\boldsymbol{l}^* = \min\{\boldsymbol{x}^{(1)}, \boldsymbol{x}^{(2)}\}$ and $\boldsymbol{u}^* = \max\{\boldsymbol{x}^{(1)}, \boldsymbol{x}^{(2)}\}$, then optimized using a multi-objective evolutionary algorithm (MOEA) [64] to yield an initial approximation of the Pareto set, with selected designs further refined using output space mapping [65]. Limiting the surrogate modeling process to $[\boldsymbol{l}^* \ \boldsymbol{u}^*]$, which provides an estimation of the Pareto front allocation in the parameter space, allows for alleviating the curse of dimensionality to a certain extent.

The cost of this procedure is 1433 EM antenna simulations, a large part of which has been generated by constructing the surrogate model (acquisition of the training data). In this case, 1000 samples were used to ensure that the model predictive power is sufficient for the design purposes (average root mean square (RMS) error of 7.7 percent). Thus, the computational savings due to the method of Section II are as high as sixty percent.

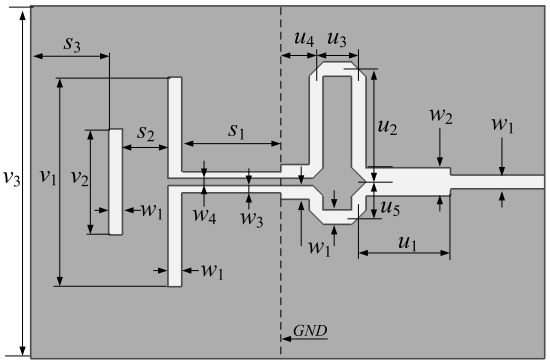

FIGURE 6. Geometry of the planar Yagi antenna [66].

B. EXAMPLE 2: PLANAR YAGI ANTENNA

The second illustration example is a planar Yagi antenna [66] shown in Fig. 6, implemented on RT6010 substrate ($\varepsilon_r = 10.2$, $h = 0.635$ mm). The designable variables are $\boldsymbol{x} = [s_1 \ s_2 \ v_1 \ v_2 \ u_1 \ u_2 \ u_3 \ u_4]^T$, whereas $w_1 = w_3 = w_4 = 0.6$, $w_2 = 1.2$, $u_5 = 1.5$, $s_3 = 3.0$, and $v_3 = 17.5$, are fixed (all dimensions in mm). The EM simulation model is implemented in CST Microwave Studio and evaluated using its time domain solver (~600,000 mesh cells, simulation time 4 minutes).

The antenna is supposed to operate in the frequency range from $f_1 = 10$ GHz to $f_2 = 11$ GHz. We consider two design objectives: (i) minimization of the in-band reflection within $[f_1 f_2]$ (F_1), and (ii) maximization of the average end-fire gain, also within $[f_1 \ f_2]$ (F_2). The single-objective optima have been found using trust-region gradient search: $\boldsymbol{x}^{(1)} = [4.38 \ 3.56 \ 8.90 \ 4.16 \ 4.08 \ 4.74 \ 2.15 \ 1.50]^T$ (maximum matching design), and $\boldsymbol{x}^{(2)} = [5.19 \ 6.90 \ 7.10 \ 5.08 \ 3.54 \ 4.78 \ 2.23 \ 0.93]^T$ (maximum average end-fire gain design).

Figure 7 illustrates the 10-element Pareto set obtained using the proposed methodology. The computational cost has been summarized in Table 3. The cost of generating the designs $\boldsymbol{x}^{(1)}$ and $\boldsymbol{x}^{(2)}$ is 160 EM antenna simulations, whereas the remaining expenses (acquisition of designs $\boldsymbol{x}^{(3)}$ through $\boldsymbol{x}^{(10)}$) are only 130 EM simulations. Consequently, the total cost is 290 EM antenna simulations. Figure 7 and Table 3 also provide the results obtained using the benchmark

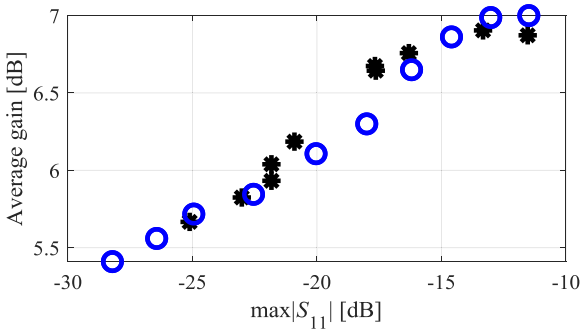

FIGURE 7. Planar Yagi antenna of Fig. 6: Pareto set found by means of the proposed methodology (o), and the set identified using the surrogate-assisted technique of [40] (*).

TABLE 2. Pareto-optimal designs for UWB antenna of Fig. 3.

	$x^{(1)}$	$x^{(2)}$	$x^{(3)}$	$x^{(4)}$	$x^{(5)}$	$x^{(6)}$	$x^{(7)}$	$x^{(8)}$	$x^{(9)}$	$x^{(10)}$
Design Variables [mm] L_g	9.81	9.95	9.66	9.51	9.49	9.39	9.36	9.37	9.21	9.07
L_0	13.26	13.48	13.15	13.07	13.22	13.32	13.41	13.32	13.28	13.39
L_s	7.82	7.90	8.21	8.40	8.82	9.02	9.31	9.69	9.90	9.93
W_s	0.23	0.36	0.21	0.32	0.26	0.26	0.31	0.42	0.37	0.43
d	4.36	3.68	3.64	3.48	3.10	2.70	2.26	2.24	2.02	2.03
dL	0.00	0.43	2.00	2.96	4.37	5.20	6.17	7.12	7.90	9.17
d_s	0.97	0.78	0.80	0.81	0.80	0.67	0.57	0.64	0.62	0.80
dW_s	1.20	1.50	1.49	1.50	1.66	1.81	1.98	2.03	2.15	2.29
dW	0.00	0.08	0.62	0.93	1.43	1.66	1.97	2.28	2.55	3.02
a	0.80	0.79	0.69	0.64	0.54	0.52	0.47	0.42	0.38	0.29
b	0.62	0.62	0.60	0.60	0.58	0.58	0.59	0.55	0.57	0.59
max $\|S_{11}\|$ [dB]	–9.3	–9.7	–10.4	–11.0	–11.6	–12.1	–12.6	–13.2	–13.6	–14.0
Area [mm^2]	166	176	207	230	261	293	324	367	400	461

(surrogate-assisted framework [40]). For the latter, the kriging surrogate constructed in the interval $[\boldsymbol{l}^*\ \boldsymbol{u}^*]$ with $\boldsymbol{l}^* = \min\{\boldsymbol{x}^{(1)}, \boldsymbol{x}^{(2)}\}$ and $\boldsymbol{u}^* = \max\{\boldsymbol{x}^{(1)}, \boldsymbol{x}^{(2)}\}$, was optimized using MOEA, and the selected designs were further refined to yield the final Pareto set. The cost of this procedure is 1190 EM antenna simulations, with as much as 1000 samples required to construct a reliable metamodel (average RMS error of 3.8 and 3.6 percent for the antenna reflection and gain, respectively). Thus, the computational savings due to the proposed approach are almost seventy percent.

Similarly as for the first example, the methodology proposed in this work allows for obtaining a uniform coverage of the Pareto front, which is not the case for the benchmark method. Furthermore, the span of the Pareto front representation rendered by the benchmark technique is narrower than for the approach presented here. Table 4 provides objective and geometry parameter values for the obtained trade-off solutions. The reflection and gain characteristic for the selected designs can be found in Fig. 8.

TABLE 3. Planar Yagi antenna of Fig. 6: optimization cost and benchmarking.

This work (inverse modeling & refinement)		Surrogate-assisted procedure [40] (benchmark)	
Cost item	Cost#	Cost item	Cost#
Single-objective optimization runs (designs $\boldsymbol{x}^{(1)}$ and $\boldsymbol{x}^{(2)}$)	$160 \times \boldsymbol{R}$	Single-objective optimization runs (designs $\boldsymbol{x}^{(1)}$ and $\boldsymbol{x}^{(2)}$)	$160 \times \boldsymbol{R}$
		Data acquisition for kriging surrogate	$1000 \times \boldsymbol{R}$
Design refinement	$130 \times \boldsymbol{R}$	MOEA optimization*	N/A
		Design refinement	$30 \times \boldsymbol{R}$
Total cost#	$290 \times \boldsymbol{R}$ (19.5 h)	Total cost#	$1190 \times \boldsymbol{R}$ (80 h)

* The cost of MOEA optimization is negligible compared to other stages of the process.
# The cost is expressed in terms of the equivalent number of EM simulations (marked as $\times \boldsymbol{R}$).

TABLE 4. Pareto-optimal designs for Yagi antenna of Fig. 6.

	$x^{(1)}$	$x^{(2)}$	$x^{(3)}$	$x^{(4)}$	$x^{(5)}$	$x^{(6)}$	$x^{(7)}$	$x^{(8)}$	$x^{(9)}$	$x^{(10)}$
Design Variables [mm] s_1	5.19	5.25	4.91	4.80	4.86	4.76	4.64	4.48	4.39	4.38
s_2	6.90	7.14	6.43	5.93	4.86	4.71	4.26	4.23	3.94	3.56
v_1	7.1	7.12	7.5	7.76	8.11	8.26	8.49	8.6	8.75	8.9
v_2	5.08	4.94	4.86	4.71	4.51	4.42	4.32	4.14	4.1	4.16
u_1	3.54	3.53	3.79	3.87	3.84	3.95	3.97	3.99	4.02	4.08
u_2	4.78	4.88	4.81	4.8	4.73	4.76	4.74	4.79	4.78	4.74
u_3	2.23	2.13	2.29	2.25	2.3	2.22	2.22	2.14	2.13	2.15
u_4	0.93	0.89	1.04	1.24	1.33	1.38	1.42	1.5	1.52	1.5
max $\|S_{11}\|$ [dB]	–11.4	–13.0	–14.6	–16.2	–18.0	–20.0	–22.5	–24.9	–26.4	–28.2
Gain* [dB]	7.0	7.0	6.9	6.7	6.3	6.1	5.8	5.7	5.6	5.4

* End-fire gain averaged over the 10-to-11 GHz bandwidth.

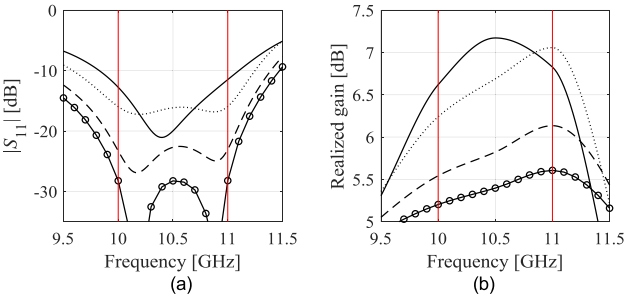

FIGURE 8. Planar Yagi antenna of Fig. 6: (a) reflection, and (b) end-fire gain characteristics for the selected Pareto designs of Table 4: $\mathbf{x^{(1)}}$ (–), $\mathbf{x^{(4)}}$ (· · ·), $\mathbf{x^{(7)}}$ (- - -), and $\mathbf{x^{(10)}}$ (-o-).

C. EXAMPLE 3: UWB MONOPOLE ANTENNA

Our last example is a UWB monopole antenna [67] shown in Fig. 9, realized on RF-35 substrate ($\varepsilon_r = 3.5$, $h = 0.762$ mm). The designable parameters are $\boldsymbol{x} = [L_0\ dR\ Rr_{rel}\ dL\ dw\ L_gL_1\ R_1\ dr\ c_{rel}]^T$. The computational model is implemented in CST Microwave Studio and evaluated using its transient solver (~840,000 mesh cells, simulation

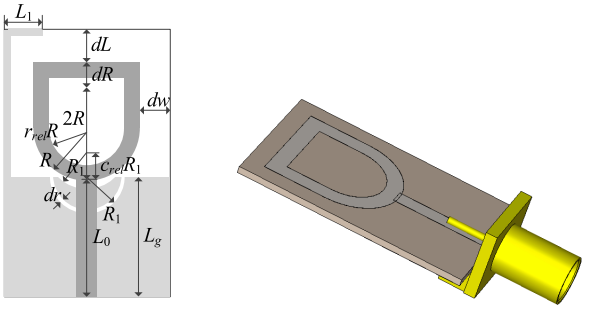

FIGURE 9. Ultra-wideband monopole antenna [67]: (a) structure geometry with the ground plane marked using the light gray shade, (b) perspective view.

TABLE 5. UWB monopole antenna of Fig. 9: optimization cost and benchmarking.

This work (inverse modeling & refinement)		Surrogate-assisted procedure [40] (benchmark)	
Cost item	Cost#	Cost item	Cost#
Single-objective optimization runs (designs $\boldsymbol{x}^{(1)}$ and $\boldsymbol{x}^{(2)}$)	$440 \times \boldsymbol{R}$	Single-objective optimization runs (designs $\boldsymbol{x}^{(1)}$ and $\boldsymbol{x}^{(2)}$)	$440 \times \boldsymbol{R}$
		Data acquisition for kriging surrogate	$1600 \times \boldsymbol{R}$
Design refinement	$242 \times \boldsymbol{R}$	MOEA optimization*	N/A
		Design refinement	$36 \times \boldsymbol{R}$
Total cost#	$682 \times \boldsymbol{R}$ (57 h)	Total cost#	$2076 \times \boldsymbol{R}$ (173 h)

* The cost of MOEA optimization is negligible compared to other stages of the process.
# The cost is expressed in terms of the equivalent number of EM simulations (marked as $\times \boldsymbol{R}$).

time 5 minutes). The model incorporates the SMA connector. The antenna is to operate from 3.1 GHz to 10.6 GHz. In the multi-objective optimization process, we consider three criteria: minimization of the in-band reflection (F_1), reduction of the realized gain variability within the operating frequency range (F_2), and reduction of the antenna footprint (F_3).

The extreme Pareto-optimal designs have been found using gradient search. We have: $\boldsymbol{x}^{(1)} = [10.64\ 0.0\ 6.00\ 0.10\ 1.46\ 6.20\ 10.46\ 4.26\ 2.00\ 0.73\ 0.49]^T$ (best matching design), $\boldsymbol{x}^{(2)} = [8.74\ 1.55\ 5.81\ 0.51\ 0.016\ 5.65\ 8.95\ 5.47\ 2.60\ 0.99\ 0.84]^T$ (minimum gain variation design), and $\boldsymbol{x}^{(3)} = [9.51\ 0.19\ 4.46\ 0.27\ 4.33\ 1.17\ 10.05\ 6.00\ 2.94\ 0.99\ 0.90]^T$ (minimum-size design).

The 15-element Pareto set generated by means of the proposed approach has been shown in Fig. 10. The cost breakdown of the optimization procedure can be found in Table 5. The overall cost of finding the design $\boldsymbol{x}^{(1)}$ through $\boldsymbol{x}^{(3)}$ is 440 antenna simulations. The cost of identifying the remaining twelve designs ($\boldsymbol{x}^{(4)}$ through $\boldsymbol{x}^{(15)}$) is only 242 EM simulations. The total expenses amount to 684 EM simulations. For the sake of comparison, Fig. 10 and Table 5 also provide the results obtained using the benchmark. The kriging surrogate model constructed for the latter in the interval

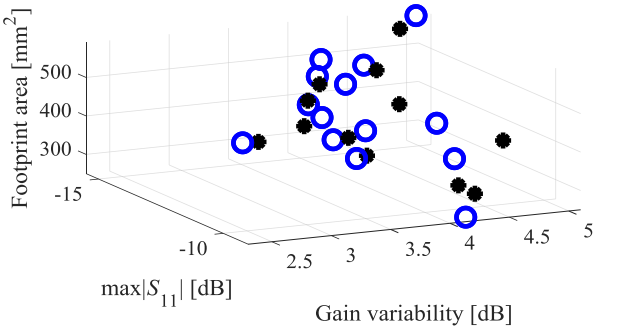

FIGURE 10. Ultra-wideband monopole antenna of Fig. 9: Pareto set found by means of the proposed methodology (o), and the set identified using the surrogate-assisted technique of [40] (*).

TABLE 6. Pareto-optimal designs for UWB monopole antenna of Fig. 9.

	Design Variables [mm]												
	L_0	dR	R	r_{rel}	dL	dw	L_g	L_1	R_1	dr	L_0	dR	R
$\boldsymbol{x}^{(1)}$	9.51	0.19	4.47	0.27	4.33	1.17	10.05	6	2.84	9.51	0.19	4.47	0.27
$\boldsymbol{x}^{(2)}$	9.14	0.31	4.92	0.66	2.52	3.4	9.54	5.98	2.65	9.14	0.31	4.92	0.66
$\boldsymbol{x}^{(3)}$	9.43	0	5.19	0.73	2.03	3.7	9.65	6	2.59	9.43	0	5.19	0.73
$\boldsymbol{x}^{(4)}$	9.37	0	5.05	0.76	2.17	3.93	9.33	6	3.05	9.37	0	5.05	0.76
$\boldsymbol{x}^{(5)}$	9.25	0.38	4.98	0.71	2.19	4.28	9.5	6	2.67	9.25	0.38	4.98	0.71
$\boldsymbol{x}^{(6)}$	9.7	0.01	4.9	0.1	3.14	4.49	9.74	5.57	2.28	9.7	0.01	4.9	0.1
$\boldsymbol{x}^{(7)}$	9.46	0.07	5.02	0.29	2.66	4.71	9.51	5.89	2.33	9.46	0.07	5.02	0.29
$\boldsymbol{x}^{(8)}$	9.54	0.09	5.18	0.2	2.42	4.85	9.65	5.76	2.28	9.54	0.09	5.18	0.2
$\boldsymbol{x}^{(9)}$	9.46	0.62	5.44	0.25	1.2	5.59	9.44	5.45	2.13	9.46	0.62	5.44	0.25
$\boldsymbol{x}^{(10)}$	8.74	1.55	5.81	0.51	0.02	5.65	8.95	5.47	2.6	8.74	1.55	5.81	0.51
$\boldsymbol{x}^{(11)}$	9.46	0.06	5.73	0.28	1.58	5.39	9.44	5.11	2.15	9.46	0.06	5.73	0.28
$\boldsymbol{x}^{(12)}$	9.86	0.01	5.41	0.31	2.03	5.67	9.76	5.08	2.14	9.86	0.01	5.41	0.31
$\boldsymbol{x}^{(13)}$	9.59	0	5.83	0.14	0.91	5.76	9.41	5.05	2	9.59	0	5.83	0.14
$\boldsymbol{x}^{(14)}$	9.76	0	5.98	0.31	0.64	5.98	9.75	5	2.02	9.76	0	5.98	0.31
$\boldsymbol{x}^{(15)}$	10.64	0	6	0.1	1.46	6.2	10.46	4.26	2	10.64	0	6	0.1

$[\boldsymbol{l}^*\ \boldsymbol{u}^*]$ with $\boldsymbol{l}^* = \min\{\boldsymbol{x}^{(1)}, \boldsymbol{x}^{(2)}, \boldsymbol{x}^{(3)}\}$ and $\boldsymbol{u}^* = \max\{\boldsymbol{x}^{(1)}, \boldsymbol{x}^{(2)}, \boldsymbol{x}^{(3)}\}$, was optimized using MOEA. Despite using as many as 1600 training samples, the predictive power of the surrogate is still limited, which is due to a relatively high dimensionality of the parameter space. The average relative RMS model error is 15% for reflection characteristics and 11% for the gain response. The final Pareto set was then obtained through local refinement. The total cost of this procedure is 2076 EM antenna simulations despite of rendering only twelve trade-off designs. The computational savings due to the proposed approach are almost seventy percent. Similarly as for the previous verification cases, our methodology permits obtaining a uniform coverage of the Pareto front (unlike the benchmark procedure), which is corroborated by the results shown in Fig. 10. Additionally, the Pareto front span produced by the proposed technique is wider than for the benchmark method.

TABLE 7. Pareto-optimal designs for UWB monopole antenna of Fig. 9: objective values.

	max $\|S_{11}\|$ [dB]	Gain variability [dB]	Footprint area [mm^2]
$\boldsymbol{x}^{(1)}$	–9.2	4.2	255
$\boldsymbol{x}^{(2)}$	–10.7	4.4	358
$\boldsymbol{x}^{(3)}$	–10.7	3.6	383
$\boldsymbol{x}^{(4)}$	–8.7	3.7	383
$\boldsymbol{x}^{(5)}$	–11.9	3.6	398
$\boldsymbol{x}^{(6)}$	–11.7	4.4	420
$\boldsymbol{x}^{(7)}$	–11.4	3.8	427
$\boldsymbol{x}^{(8)}$	–12.3	3.6	444
$\boldsymbol{x}^{(9)}$	–12.3	3.5	482
$\boldsymbol{x}^{(10)}$	–9.6	2.4	495
$\boldsymbol{x}^{(11)}$	–13.1	4	495
$\boldsymbol{x}^{(12)}$	–14.4	4.4	497
$\boldsymbol{x}^{(13)}$	–13.6	3.8	507
$\boldsymbol{x}^{(14)}$	–14.2	4	528
$\boldsymbol{x}^{(15)}$	–15.2	5	581

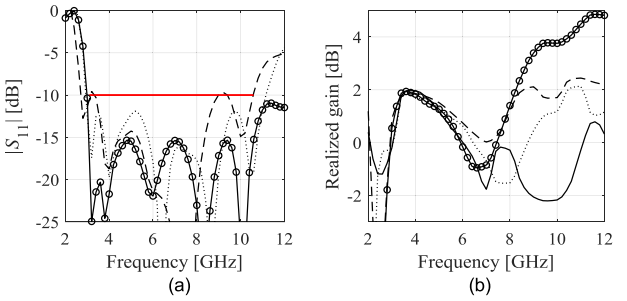

FIGURE 11. Ultra-wideband monopole antenna of Fig. 9: (a) reflection, and (b) end-fire gain characteristics for the selected Pareto designs of Table 6: $\boldsymbol{x}^{(1)}$ (–), $\boldsymbol{x}^{(5)}$ (· · ·), $\boldsymbol{x}^{(10)}$ (- - -), and $\boldsymbol{x}^{(15)}$ (-o-).

Again, the methodology proposed in this paper allows for obtaining a relatively uniform coverage of the Pareto front. The span of the Pareto front representation rendered by both methods is similar. Tables 6 and 7 provide geometry parameter and objective values, respectively, for the obtained trade-off solutions. The reflection and gain characteristic for the selected designs have been shown in Fig. 11.

IV. CONCLUSION

The paper proposed a novel deterministic machine learning framework for multi-objective optimization of antenna structures. Our methodology relies on a sequential rendition of the Pareto-optimal designs based on triangulation of the already accumulated knowledge in the form of Pareto set representation, as well as a supplementary surrogate-assisted refinement procedure. The algorithm does not involve any stochastic search methods such as population-based metaheuristics. It has been comprehensively validated using three examples of microstrip antennas featuring distinct types of responses, and optimized with respect to various criteria such as matching improvement, size reduction, or minimization of the in-band gain variability. It has been demonstrated that the presented technique allows for generating trade-off solutions that uniformly cover the Pareto fronts of the respective structures. Meanwhile, the computational cost of the optimization process is low and corresponds to a few hundreds of EM antenna simulations, with the average expenses of about forty simulations per trade-off design, but only fifteen simulations per design for the core part of the algorithm (i.e., excluding acquisition of the extreme Pareto-optimal points). The computational savings over the state-of-the-art surrogate-assisted technique are as high as seventy percent, while ensuring broader and more uniform coverage of the front.

One of the practical limitations of the presented approach is the number of design objectives that can be efficiently handled. Although there are no formal restrictions, due to the triangulation process involved in the procedure, uniformity of the trade-off design allocation is slightly degraded already at three objectives, and is expected to further deteriorate beyond that number. Notwithstanding, the proposed methodology may be a viable alternative to the existing techniques for rapid two- or three-objective optimization, especially in the context of compact antennas (e.g., impedance matching, gain, or axial ratio versus footprint area).

ACKNOWLEDGMENT

The authors would like to thank Dassault Systemes, France, for making CST Microwave Studio available.

REFERENCES

[1] Q. Wu, J. Yin, C. Yu, H. Wang, and W. Hong, "Broadband planar SIW cavity-backed slot antennas aided by unbalanced shorting vias," *IEEE Antennas Wireless Propag. Lett.*, vol. 18, no. 2, pp. 363–367, Feb. 2019.

[2] G. Yang, S. Zhang, J. Li, Y. Zhang, and G. F. Pedersen, "A multi-band magneto-electric dipole antenna with wide beam-width," *IEEE Access*, vol. 8, pp. 68820–68827, 2020.

[3] R. Hussain, M. U. Khan, and M. S. Sharawi, "An integrated dual MIMO antenna system with dual-function GND-plane frequency-agile antenna," *IEEE Antennas Wireless Propag. Lett.*, vol. 17, no. 1, pp. 142–145, Jan. 2018.

[4] A.-S. Kaddour, S. Bories, A. Bellion, and C. Delaveaud, "3-D-printed compact wideband magnetoelectric dipoles with circular polarization," *IEEE Antennas Wireless Propag. Lett.*, vol. 17, no. 11, pp. 2026–2030, Nov. 2018.

[5] L.-R. Tan, R.-X. Wu, and Y. Poo, "Magnetically reconfigurable SIW antenna with tunable frequencies and polarizations," *IEEE Trans. Antennas Propag.*, vol. 63, no. 6, pp. 2772–2776, Jun. 2015.

[6] N. Yang and K. W. Leung, "Compact cylindrical pattern-diversity dielectric resonator antenna," *IEEE Antennas Wireless Propag. Lett.*, vol. 19, no. 1, pp. 19–23, Jan. 2020.

[7] S. Zhu, H. Liu, Z. Chen, and P. Wen, "A compact gain-enhanced vivaldi antenna array with suppressed mutual coupling for 5G mmWave application," *IEEE Antennas Wireless Propag. Lett.*, vol. 17, no. 5, pp. 776–779, May 2018.

[8] G.-P. Gao, C. Yang, B. Hu, R.-F. Zhang, and S.-F. Wang, "A wide-bandwidth wearable all-textile PIFA with dual resonance modes for 5 GHz WLAN applications," *IEEE Trans. Antennas Propag.*, vol. 67, no. 6, pp. 4206–4211, Jun. 2019.

[9] J. Wang, M. Leach, E. G. Lim, Z. Wang, R. Pei, and Y. Huang, "An implantable and conformal antenna for wireless capsule endoscopy," *IEEE Antennas Wireless Propag. Lett.*, vol. 17, no. 7, pp. 1153–1157, Jul. 2018.

[10] Z. Ren, A. Zhao, and S. Wu, "MIMO antenna with compact decoupled antenna pairs for 5G mobile terminals," *IEEE Antennas Wireless Propag. Lett.*, vol. 18, no. 7, pp. 1367–1371, Jul. 2019.

[11] A. Zhao and Z. Ren, "Size reduction of self-isolated MIMO antenna system for 5G mobile phone applications," *IEEE Antennas Wireless Propag. Lett.*, vol. 18, no. 1, pp. 152–156, Nov. 2019.

[12] M. Ko, H. Lee, and J. Choi, "Planar LTE/sub-6 GHz 5G MIMO antenna integrated with mmWave 5G beamforming phased array antennas for V2X applications," *IET Microw., Antennas Propag.*, vol. 14, no. 11, pp. 1283–1295, Sep. 2020.

[13] T. Houret, L. Lizzi, F. Ferrero, C. Danchesi, and S. Boudaud, "DTC-enabled frequency-tunable inverted-F antenna for IoT applications," *IEEE Antennas Wireless Propag. Lett.*, vol. 19, no. 2, pp. 307–311, Feb. 2020.

[14] K. R. Jha, B. Bukhari, C. Singh, G. Mishra, and S. K. Sharma, "Compact planar multistandard MIMO antenna for IoT applications," *IEEE Trans. Antennas Propag.*, vol. 66, no. 7, pp. 3327–3336, Jul. 2018.

[15] Y.-H. Yang, B.-H. Sun, and J.-L. Guo, "A low-cost, single-layer, dual circularly polarized antenna for millimeter-wave applications," *IEEE Antennas Wireless Propag. Lett.*, vol. 18, no. 4, pp. 651–655, Apr. 2019.

[16] J.-S. Row and L.-K. Kuo, "Pattern-reconfigurable array based on a circularly polarized antenna with broadband operation and high front-to-back ratio," *IEEE Trans. Antennas Propag.*, vol. 68, no. 5, pp. 4109–4113, May 2020.

[17] Z. L. Ma, C. H. Chan, K. B. Ng, and L. J. Jiang, "A collimated surface-wave-excited high-impedance surface leaky-wave antenna," *IEEE Antennas Wireless Propag. Lett.*, vol. 16, pp. 2082–2085, 2017.

[18] S. Koziel, Q. S. Cheng, and S. Li, "Optimization-driven antenna design framework with multiple performance constraints," *Int. J. RF Microw. Comput.-Aided Eng.*, vol. 28, no. 4, May 2018, Art. no. e21208.

[19] J. Liu, K. P. Esselle, S. G. Hay, and S. Zhong, "Effects of printed UWB antenna miniaturization on pulse fidelity and pattern stability," *IEEE Trans. Antennas Propag.*, vol. 62, no. 8, pp. 3903–3910, Aug. 2014.

[20] M. Kovaleva, D. Bulger, and K. P. Esselle, "Comparative study of optimization algorithms on the design of broadband antennas," *IEEE J. Multiscale Multiphys. Comput. Techn.*, vol. 5, pp. 89–98, 2020.

[21] S. Koziel and A. Pietrenko-Dabrowska, "Expedited feature-based quasi-global optimization of multi-band antennas with Jacobian variability tracking," *IEEE Access*, vol. 8, pp. 83907–83915, 2020.

[22] T. G. Kolda, R. M. Lewis, and V. Torczon, "Optimization by direct search: New perspectives on some classical and modern methods," *SIAM Rev.*, vol. 45, no. 3, pp. 385–482, Jan. 2003.

[23] M. John and M. J. Ammann, "Antenna optimization with a computationally efficient multiobjective evolutionary algorithm," *IEEE Trans. Antennas Propag.*, vol. 57, no. 1, pp. 260–263, Jan. 2009.

[24] W.-J. Zhao, E.-X. Liu, B. Wang, S.-P. Gao, and C. E. Png, "Differential evolutionary optimization of an equivalent dipole model for electromagnetic emission analysis," *IEEE Trans. Electromagn. Compat.*, vol. 60, no. 6, pp. 1635–1639, Dec. 2018.

[25] A. Lalbakhsh, M. U. Afzal, and K. P. Esselle, "Multiobjective particle swarm optimization to design a time-delay equalizer metasurface for an electromagnetic band-gap resonator antenna," *IEEE Antennas Wireless Propag. Lett.*, vol. 16, pp. 912–915, 2017.

[26] P. Baumgartner, T. Bauernfeind, O. Biro, A. Hackl, C. Magele, W. Renhart, and R. Torchio, "Multi-objective optimization of Yagi–Uda antenna applying enhanced firefly algorithm with adaptive cost function," *IEEE Trans. Magn.*, vol. 54, no. 3, Mar. 2018, Art. no. 8000504.

[27] R. T. Marler and J. S. Arora, "The weighted sum method for multi-objective optimization: New insights," *Struct. Multidisciplinary Optim.*, vol. 41, no. 6, pp. 853–862, Jun. 2010.

[28] F. W. Gembicki, "Vector optimization for control with performance and parameter sensitivity indices," Ph.D. dissertation, Case Wester Reserve Univ., Cleveland, OH, USA, 1974.

[29] U. Ullah, S. Koziel, and I. B. Mabrouk, "Rapid redesign and Bandwidth/Size tradeoffs for compact wideband circular polarization antennas using inverse surrogates and fast EM-based parameter tuning," *IEEE Trans. Antennas Propag.*, vol. 68, no. 1, pp. 81–89, Jan. 2020.

[30] S. Mirjalili, and J. S. Dong, *Multi-Objective Optimization using Artificial Intelligence Techniques*. New York, NY, USA: Springer, 2019.

[31] J. K. Mandal, S. Mukhopadhyay, and P. Dutta, *Multi-Objective Optimization: Evolutionary to Hybrid Framework*. New York, NY, USA: Springer, 2018.

[32] S. Chamaani, S. A. Mirtaheri, and M. S. Abrishamian, "Improvement of time and frequency domain performance of antipodal vivaldi antenna using multi-objective particle swarm optimization," *IEEE Trans. Antennas Propag.*, vol. 59, no. 5, pp. 1738–1742, May 2011.

[33] R. Carvalho, R. R. Saldanha, B. N. Gomes, A. C. Lisboa, and A. X. Martins, "A multi-objective evolutionary algorithm based on decomposition for optimal design of Yagi-Uda antennas," *IEEE Trans. Magn.*, vol. 48, no. 2, pp. 803–806, Feb. 2012.

[34] S. K. Goudos, K. A. Gotsis, K. Siakavara, E. E. Vafiadis, and J. N. Sahalos, "A multi-objective approach to subarrayed linear antenna arrays design based on memetic differential evolution," *IEEE Trans. Antennas Propag.*, vol. 61, no. 6, pp. 3042–3052, Jun. 2013.

[35] Y. Zhang, X. Liu, F. Bao, J. Chi, C. Zhang, and P. Liu, "Particle swarm optimization with adaptive learning strategy," *Knowl.-Based Syst.*, vol. 196, May 2020, Art. no. 105789.

[36] S. Maddio, G. Pelosi, M. Righini, and S. Selleri, "A multi-objective invasive weed optimization for broad band sequential rotation networks," in *Proc. IEEE Int. Symp. Antennas Propag. USNC/URSI Nat. Radio Sci. Meeting*, Boston, MA, USA, Jul. 2018, pp. 955–956.

[37] D. Z. Zhu, P. L. Werner, and D. H. Werner, "Multi-objective lazy ant colony optimization for frequency selective surface design," in *Proc. IEEE Int. Symp. Antennas Propag. USNC/URSI Nat. Radio Sci. Meeting*, Boston, MA, USA, Jul. 2018, pp. 2035–2036.

[38] P. Ranjan, S. K. Mahto, and A. Choubey, "BWDO algorithm and its application in antenna array and pixelated metasurface synthesis," *IET Microw., Antennas Propag.*, vol. 13, no. 9, pp. 1263–1270, Jul. 2019.

[39] C. Zhang, X. Fu, S. Peng, Y. Wang, and J. Chang, "New multi-objective optimisation algorithm for uniformly excited aperiodic array synthesis," *IET Microw., Antennas Propag.*, vol. 13, no. 2, pp. 171–177, Feb. 2019.

[40] S. Koziel and A. Bekasiewicz, *Multi-Objective Design of Antennas Using Surrogate Models*. Singapore: World Scientific, 2016.

[41] Y. Zhao, C. Sun, J. Zeng, Y. Tan, and G. Zhang, "A surrogate-ensemble assisted expensive many-objective optimization," *Knowl.-Based Syst.*, vol. 211, Jan. 2021, Art. no. 106520.

[42] D. I. L. de Villiers, I. Couckuyt, and T. Dhaene, "Multi-objective optimization of reflector antennas using kriging and probability of improvement," in *Proc. IEEE Int. Symp. Antennas Propag. USNC/URSI Nat. Radio Sci. Meeting*, San Diego, CA, USA, Jul. 2017, pp. 985–986.

[43] S. Koziel and S. Ogurtsov, "Multi-objective design of antennas using variable-fidelity simulations and surrogate models," *IEEE Trans. Antennas Propag.*, vol. 61, no. 12, pp. 5931–5939, Dec. 2013.

[44] J. A. Easum, J. Nagar, P. L. Werner, and D. H. Werner, "Efficient multiobjective antenna optimization with tolerance analysis through the use of surrogate models," *IEEE Trans. Antennas Propag.*, vol. 66, no. 12, pp. 6706–6715, Dec. 2018.

[45] S. Xiao, G. Q. Liu, K. L. Zhang, Y. Z. Jing, J. H. Duan, P. Di Barba, and J. K. Sykulski, "Multi-objective Pareto optimization of electromagnetic devices exploiting kriging with lipschitzian optimized expected improvement," *IEEE Trans. Magn.*, vol. 54, no. 3, Mar. 2018, Art. no. 7001704.

[46] A. I. J. Forrester and A. J. Keane, "Recent advances in surrogate-based optimization," *Prog. Aerosp. Sci.*, vol. 45, nos. 1–3, pp. 50–79, Jan. 2009.

[47] B. Xia, Z. Ren, and C.-S. Koh, "Utilizing kriging surrogate models for multi-objective robust optimization of electromagnetic devices," *IEEE Trans. Magn.*, vol. 50, no. 2, pp. 693–696, Feb. 2014.

[48] J. P. Jacobs, "Characterisation by Gaussian processes of finite substrate size effects on gain patterns of microstrip antennas," *IET Microw., Antennas Propag.*, vol. 10, no. 11, pp. 1189–1195, Aug. 2016.

[49] Z. Lv, L. Wang, Z. Han, J. Zhao, and W. Wang, "Surrogate-assisted particle swarm optimization algorithm with Pareto active learning for expensive multi-objective optimization," *IEEE/CAA J. Automatica Sinica*, vol. 6, no. 3, pp. 838–849, May 2019.

[50] S. Koziel and A. Pietrenko-Dabrowska, "Performance-based nested surrogate modeling of antenna input characteristics," *IEEE Trans. Antennas Propag.*, vol. 67, no. 5, pp. 2904–2912, May 2019.

[51] S. Koziel and A. T. Sigurðsson, "Multi-fidelity EM simulations and constrained surrogate modelling for low-cost multi-objective design optimisation of antennas," *IET Microw., Antennas Propag.*, vol. 12, no. 13, pp. 2025–2029, Oct. 2018.

[52] S. Koziel and A. Pietrenko-Dabrowska, "Rapid multi-objective optimization of antennas using nested kriging surrogates and single-fidelity EM simulation models," *Eng. Comput.*, vol. 37, no. 4, pp. 1491–1512, Dec. 2019.

[53] S. Koziel and P. Kurgan, "Rapid multi-objective design of integrated on-chip inductors by means of Pareto front exploration and design extrapolation," *J. Electromagn. Waves Appl.*, vol. 33, no. 11, pp. 1416–1426, Jul. 2019.
[54] S. Koziel and A. Bekasiewicz, "Pareto-ranking bisection algorithm for expedited multiobjective optimization of antenna structures," *IEEE Antennas Wireless Propag. Lett.*, vol. 16, pp. 1488–1491, 2017.
[55] A. Amrit, L. Leifsson, and S. Koziel, "Fast multi-objective aerodynamic optimization using sequential domain patching and multifidelity models," *J. Aircr.*, vol. 57, no. 3, pp. 388–398, May 2020.
[56] S. D. Unnsteinsson and S. Koziel, "Generalized Pareto ranking bisection for computationally feasible multiobjective antenna optimization," *Int. J. RF Microw. Comput.-Aided Eng.*, vol. 28, no. 8, Oct. 2018, Art. no. e21406.
[57] Y. Liu, Q. S. Cheng, and S. Koziel, "A generalized SDP multi-objective optimization method for EM-based microwave device design," *Sensors*, vol. 19, no. 14, p. 3065, 2019.
[58] K. Deb, *Multi-Objective Optimization Using Evolutionary Algorithms*. New York, NY, USA: Wiley, 2001.
[59] A. Amrit, L. Leifsson, and S. Koziel, "Multi-fidelity aerodynamic design trade-off exploration using point-by-point Pareto set identification," *Aerosp. Sci. Technol.*, vol. 79, pp. 399–412, Aug. 2018.
[60] H. Borouchaki, P. L. George, and S. H. Lo, "Optimal delaunay point insertion," *Int. J. Numer. Methods Eng.*, vol. 39, no. 20, pp. 3407–3437, Oct. 1996.
[61] C. G. Broyden, "A class of methods for solving nonlinear simultaneous equations," *Math. Comput.*, vol. 19, no. 92, pp. 577–593, 1965.
[62] M. A. U. Haq and S. Koziel, "Simulation-based optimization for rigorous assessment of ground plane modifications in compact UWB antenna design," *Int. J. RF Microw. Comput.-Aided Eng.*, vol. 28, no. 4, May 2018, Art. no. e21204.
[63] A. R. Conn, N. I. M. Gould, and P. L. Toint, "Trust region methods," in *MPS-SIAM Series on Optimization*. Philadelphia, PA, USA: SIAM, 2000.
[64] C. M. Fonseca, "Multiobjective genetic algorithms with application to control engineering problems," Ph.D. dissertation, Dept. Autom. Control Syst. Eng., Univ. Sheffield, Sheffield, U.K., 1995.
[65] S. Koziel, Q. S. Cheng, and J. W. Bandler, "Space mapping," *IEEE Microw. Mag.*, vol. 9, no. 6, pp. 105–122, Dec. 2008.
[66] N. Kaneda, W. R. Deal, Y. Qian, R. Waterhouse, and T. Itoh, "A broadband planar Quasi-Yagi antenna," *IEEE Trans. Antennas Propag.*, vol. 50, no. 8, pp. 1158–1160, Aug. 2002.
[67] M. G. N. Alsath and M. Kanagasabai, "Compact UWB monopole antenna for automotive communications," *IEEE Trans. Antennas Propag.*, vol. 63, no. 9, pp. 4204–4208, Sep. 2015.

SLAWOMIR KOZIEL (Senior Member, IEEE) received the M.Sc. and Ph.D. degrees in electronic engineering from the Gdańsk University of Technology, Poland, in 1995 and 2000, respectively, the M.Sc. degree in theoretical physics and the M.Sc. degree in mathematics, in 2000 and 2002, respectively, and the Ph.D. degree in mathematics from the University of Gdańsk, Poland, in 2003. He is currently a Professor with the Department of Engineering, Reykjavik University, Iceland. His research interests include CAD and modeling of microwave and antenna structures, simulation-driven design, surrogate-based optimization, space mapping, circuit theory, analog signal processing, evolutionary computation, and numerical analysis.

ANNA PIETRENKO-DABROWSKA (Senior Member, IEEE) received the M.Sc. and Ph.D. degrees in electronic engineering from the Gdańsk University of Technology, Poland, in 1998 and 2007, respectively. She is currently an Associate Professor with the Gdańsk University of Technology. Her research interests include simulation-driven design, design optimization, control theory, modeling of microwave and antenna structures, and numerical analysis.